Hindawi
Structural Control and Health Monitoring
Volume 2024, Article ID 1710019, 15 pages
https://doi.org/10.1155/2024/1710019

Research Article

Innovative Approach to Dam Deformation Analysis: Integration of VMD, Fractal Theory, and WOA-DELM

Bin Ou,[1,2,3] **Caiyi Zhang**,[1,2] **Bo Xu**,[4] **Shuyan Fu**,[1,2] **Zhenyu Liu**,[1,2] **and Kui Wang**[1,2]

[1]*College of Water Conservancy, Yunnan Agricultural University, Kunming, China*
[2]*Yunnan Province Small and Medium-Sized Water Conservancy Project Intelligent Management and Maintenance Engineering Research Center, Kunming, China*
[3]*The National Key Laboratory of Water Disaster Prevention, Nanjing, China*
[4]*College of Hydraulic Science and Engineering, Yangzhou University, Yangzhou, China*

Correspondence should be addressed to Bo Xu; xubo@yzu.edu.cn

Received 25 November 2023; Revised 24 April 2024; Accepted 8 May 2024; Published 20 May 2024

Academic Editor: Sara Casciati

This paper introduces a novel and comprehensive model for the analysis of dam deformation trends, integrating the variational mode decomposition (VMD) method, fractal theory, and the whale optimization algorithm (WOA) to refine the deep extreme learning machine (DELM) model. This integration allows for a meticulous denoising process through VMD, effectively isolating pertinent signal characteristics from noise and measurement interference. Following this, fractal theory is utilized to conduct an in-depth qualitative analysis of the denoised data, capturing intricate patterns within the deformation trends. The model further evolves with the application of WOA to optimize the DELM model, thereby facilitating an integrated approach that merges qualitative insights with quantitative analysis. The efficacy of this advanced model is demonstrated through a case study, highlighting its capability to deliver accurate and reliable predictions that are in harmony with practical engineering scenarios. This research not only offers a robust framework for analyzing dam deformation trends but also sets a new standard in the field, providing a new solution for assessing structural integrity in hydrological engineering.

1. Introduction

Concrete dams are indispensable for effective water resource management and contribute significantly to national economic growth. Ensuring their operational safety demands accurate monitoring and forecasting of deformation trends [1–3]. The primary challenge in this process is the presence of noise in deformation data, which complicates the analysis. In addition, the intrinsic nonlinear characteristics of dam deformations present further difficulties in accurately estimating and predicting these trends [4, 5]. Consequently, the development of a mathematical model that correlates the deformation of dams with its influencing factors is essential for predicting trends and ensuring the structural integrity of these vital infrastructures [6, 7].

Contemporary methods for monitoring dam deformation are primarily categorized into statistical [8], deterministic [9], and hybrid models [10, 11]. While statistical models are prevalent due to their simplicity and ease of implementation, the evolution of computational technologies and intelligent algorithms, such as support vector machines [12] and neural networks, has led to their widespread adoption in this field. Addressing these complexities, researchers globally have proposed various models for dam deformation trend analysis and prediction [13, 14]. Recent advancements in computational methods such as machine learning have opened new avenues for dam deformation analysis, offering more precise and reliable predictions. For instance, Deng et al. [15] utilized the Kalman filtering method in conjunction with fractal theory and the R/S analysis method for qualitative assessment, further

developing a long short-term memory (LSTM)-based quantitative model. In addition, Hao et al. [16] employed the R/S analysis method to discern dam deformation trends and utilized an optimized extreme learning machine combined with chaos theory for effective prediction. Bui et al. [17] introduced a novel approach with the coronavirus optimization algorithm and LSTM for dam deformation prediction in hydropower plants. However, these models often focus on specific aspects of dam deformation, with limitations in handling data disturbances, employing time-dependent monitoring data, parameter determination, constructing intricate mathematical models, and predicting long-term trends. This underscores the need for a multifaceted approach, incorporating advanced theoretical methods to enhance the reliability and scope of dam deformation trend analysis.

Recognizing the complexities in dam deformation data analysis, variational mode decomposition (VMD) emerges as a pivotal method. Its efficacy in processing dam deformation data, retaining and accentuating the trend characteristics, and enhancing the authenticity and stability of information representation is well documented [18–20]. This approach is notably advanced in the model proposed by Chen et al. [21], which integrates VMD with LSTM neural networks. Their model leverages VMD for denoising dam monitoring data, followed by employing LSTM neural networks for predictive analysis, thereby significantly improving dam deformation prediction accuracy. In order to improve the prediction accuracy of nonstationary nonlinear monthly runoff series, Wang et al. [22] introduced the whale optimization algorithm (WOA) to optimize the VMD and combined it with the gated recurrent unit (GRU) and constructed the runoff prediction model of WOA-VMD-GRU. The model effectively improves the effectiveness and accuracy of monthly runoff sequence preprocessing. Xu et al. [23] proposed a coupled prediction model for improving runoff prediction, which decomposes the original runoff sequence by an improved fully ensemble empirical modal decomposition (EMD) combined with wavelet decomposition (WD) and then predicts the monthly runoff using a support vector machine (SVM) optimized by the seagull optimization algorithm (SOA). The model effectively improves the prediction accuracy of runoff.

Fractal theory, known for its ability to capture the self-similarity and scale characteristics in dam deformation data [24–26], provides an additional layer of analysis. In this vein, Xie et al. [27] utilized multifractal theory to dissect the multifractal characteristics of dam displacement time series, examining the amplitude, trend fluctuations, and their relationship with environmental variables. The application of fractal prediction principles for fitting and predicting the dam displacement time series further exemplifies the theory's utility. In addition, the whale optimization algorithm (WOA), acknowledged for its diverse search strategies and high efficiency, plays a crucial role [28–30]. When applied to optimize the deep limit learning machine model [31, 32], it significantly bolsters the model's performance and convergence speed, offering an effective solution for high-dimensional nonlinear problems.

Thus, this article introduces an integrated model combining the VMD noise reduction method, fractal theory, and WOA-DELM. It starts with decomposing the collected monitoring data using VMD, followed by analyzing the resulting intrinsic mode functions (IMFs) through fractal theory to identify the deformation trends of the dam. Building on this analysis, the deep extreme learning machine (DELM) model is selected as the foundational model. Optimizing this model with the WOA leads to the construction of the WOA-DELM dam deformation prediction model. This model's predictions are then juxtaposed with the analytical and judgment results derived from fractal theory for validation. This methodology not only accurately forecasts the future deformation trends of the dam but also provides a comprehensive understanding of its dynamic characteristics.

2. Theory and Methodology

2.1. Decomposition Using VMD. VMD is an advanced signal decomposition technique that separates an original signal into IMFs with distinct frequencies, amplitudes, and phases. This separation is achieved through a combination of regularization constraints and iterative solutions, leading to more stable and manageable decomposition outcomes [33]. In contrast to empirical modal decomposition (EMD), VMD is underpinned by a more comprehensive and robust mathematical framework, enabling it to provide more accurate decomposition results. Not only are these results more reliable and easier to control, but they are also attained with greater computational efficiency. Han et al. [34] showed that the VMD showed superior noise filtering ability under drastic fluctuations of water level in dam reservoirs as compared to EMD.

In the VMD process, the input signal undergoes modal separation, resulting in a set of IMF components through successive iterations. These IMFs denoted as $\{u_k\} = \{u_1, u_2, \cdots, u_k\}$, $k = 1, 2, \cdots, K$, are then processed through the following steps:

① For each IMF component, the associated signal is calculated using the Hilbert–Huang transform as

$$\left(\delta(t) + \frac{j}{\pi t}\right) \times u_k(t). \tag{1}$$

② The spectrum of each mode u_k is shifted to its baseband by adding an exponential term $e^{-j\omega t}$, aligning with the mode's central frequency:

$$\left[\left(\delta(t) + \frac{j}{\pi t}\right) \times u_k(t)\right] e^{-j\omega t}. \tag{2}$$

③ The demodulated signal is estimated by applying H1 Gaussian smoothing to the signal's bandwidth. This step formulates the variational constraint problem, leading to a set of defining equations:

$$\min_{\{u_k\},\{w_k\}} \left\{ \sum_k \left\| \partial_t \left[\left(\delta(t) + \frac{j}{\pi t} \right) \times u_k(t) \right] e^{-j\omega t} \right\|_2^2 \right\}. \quad (3)$$

In the VMD framework, the original signal is denoted as f, and the central frequencies of each IMF component u_k are represented by $\{\omega_k\} = \{\omega_1, \omega_2, \cdots, \omega_k\}$ for. $k = 1, 2, \cdots, K$. The notation ∂_t denotes the partial derivative and $\delta(t)$ is the Dirac function.

Addressing the variational problem, the incorporation of the Lagrange multiplier $\lambda(t)$ and the quadratic penalty factor α transforms the original constrained variational problem into an unconstrained one. This transformation is expressed as follows:

$$L\{\{u_k\},\{\omega\},\lambda\} = \alpha \sum_k \left\| \partial_t \left[\left(\delta(t) + \frac{j}{\pi t} \right) \times u_k(t) \right] e^{-j\omega t} \right\| + \left\| f(t) - \sum_k u_k(t) \right\|_2^2 + \left(\lambda(t), f(t) - \sum_k u_k(t) \right). \quad (4)$$

To solve the minimum of this problem, the alternating direction method of multipliers is utilized, involving iterative updates of u_k^{n+1}, ω_k^{n+1}, and λ^{n+1}. The formulas for these updates are structured to ensure convergence toward the solution, taking into account the contributions of each IMF component and the corresponding noise level τ:

$$\begin{aligned} u_k^{n+1}(\omega) &= \frac{f(\omega) - \sum_{i=1}^{k-1} u_1^{n+1}(\omega) - \sum_{i=k+1}^{K} u_1^n(\omega) + \lambda(\omega)/2}{1 + 2\alpha(\omega - \omega_k^n)^2}, \\ \omega_k^{n+1} &= \frac{\int_0^\infty \omega \left| u_k^{n+1}(\omega) \right|^2 d\omega}{\int_0^\infty \left| u_k^{n+1}(\omega) \right|^2 d\omega}, \\ \lambda^{n+1}(\omega) &= \lambda^n(\omega) + \tau \left[f(\omega) - \sum_k u_k^{n+1}(\omega) \right], \end{aligned} \quad (5)$$

where τ is the noise.

The specific decomposition process in VMD commences with initializing $\{u_k^1\}, \{\omega_k^1\}, \lambda^1$, and setting $n = 0$. The procedure involves an outer loop where n is incremented, and for each k (starting from 0 and incrementing to K), both the first and second inner loops are executed. During these loops, u_k and ω_k are updated according to equation (5), and λ is also updated accordingly. The process is iterative, and the condition for terminating the loop iteration is defined as follows:

$$\frac{\sum k \left\| u_k^{n+1}(\omega) - u_k^n(\omega) \right\|_2^2}{\left\| u_k^n(\omega) \right\|_2^2} < \varepsilon, \quad (6)$$

where ε is the convergence tolerance limit. Upon meeting this convergence criterion, the process yields K modal components; if not, the steps are repeated.

2.2. Fractal Theory in Signal Analysis. Fractal theory explores the intricate patterns in complex and irregular structures using simple, repetitive rules. A fractal is essentially a spatial pattern or structure, remarkable for its high self-similarity, that replicates itself consistently. Within this theoretical framework, the Katz function and the box-pin method stand out as pivotal concepts, though they are applied differently in terms of computational and practical contexts. The study by Pei et al. [35]. indicated that fractal theory has good results in dam displacement analysis and prediction.

The Katz function assesses the importance of a node in a network by measuring its relative distance from adjacent nodes [36]. This function calculates the centrality of a node as a cumulative weight of paths linking it to other nodes in the network, weighted by the alpha parameter. The magnitude of alpha plays a crucial role in determining the impact of distant paths on the node's importance, enabling adaptability to various network structures. The Katz function is typically represented as

$$\text{Katz}(v) = \text{alpha} * \text{sum}\left(\text{beat}^i \times A^i \right), \quad (7)$$

where v is the target node, alpha and beat represent specific parameters, A is the adjacency matrix, i is the path length, and A^i represents the i-th power of the adjacency matrix.

Another widely utilized technique in fractal analysis is the wavelet transform method. This time–frequency analysis approach decomposes and reconstructs a signal across various scales. Specifically, wavelet packet decomposition (WPD), a derivative of the wavelet transform, enables the decomposition of a signal into frequency-specific segments, yielding corresponding wavelet packet coefficients [37].

The WPD process begins with the selection of a suitable wavelet basis function, commonly the Daubechies wavelet basis (db4), denoted as $\varphi(t)$. The signal $x(t)$ is then

decomposed into layers of wavelet packet coefficients, each representing a different frequency content of the signal. The wavelet packet coefficients for the j-th layer, denoted as $Cj(k)$, where k indicates the subband index within the range of $[0, 2^{j-1}]$, are computed as follows:

$$Cj(k) = \int \left[x(t) * \varphi_j k(t) \right] \mathrm{d}t, \tag{8}$$

where $*$ indicates the convolution and $\varphi_j k(t)$ represents the translation and scale transformation of the wavelet basis function.

The analysis extends further by processing the wavelet packet coefficients of each layer to calculate local Hurst indices. The process involves determining the signal length N and the number of subsegments M, along with the scale range K_q. For each scale within the range K_q and based on the number of subsegments M, delta values are computed and applied to segment the wavelet packet subbands. Subsequently, local Hurst indices for each wavelet packet subband are calculated independently for each layer. The final step involves computing a weighted average of the local Hurst indices for each layer, thus providing a comprehensive fractal analysis of the signal.

2.3. Optimization Techniques with WOA. The WOA draws inspiration from the fascinating natural phenomena observed in whale behaviors [28]. This optimization algorithm is designed to mimic the hunting tactics of whales, including their search, encirclement, and predation strategies. Each whale within the algorithm is conceptualized as a search agent, and collectively, they form a dynamic search space. The whales navigate this space, constantly adjusting their positions to converge on the most favorable solution, akin to a whale pursuing its prey. WOA's simplicity, ease of understanding, and adaptability make it suitable for a wide array of optimization problems. WOA has shown significant efficiency in optimizing the parameters of dam deformation prediction models, as evidenced by the study of Wang et al. [38]. The specific whale algorithm is shown schematically in Figure 1. Its operational mechanics are outlined as follows [39].

The WOA consists of several key aspects which are as follows:

(1) Bracketing phase

This phase involves calculating the distance D between the current position $X(t)$ and the optimal position $X_P(t)$, which represents the whale's encirclement of its target. The distance is defined as follows:

$$D = \left| C \cdot X_P(t) - X(t) \right|, \tag{9}$$

where $X_P(t)$ is the optimal position, $X(t)$ is the current position, t is the iteration count, C is the perturbation factor, and D is the updating step during the encirclement phase.

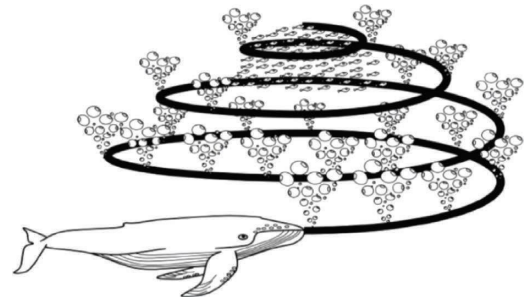

Figure 1: Illustration of the whale optimization algorithm.

The process of updating individual positions within the WOA is methodically formulated. The position at the next iteration, $X(t+1)$, is determined by the following equation:

$$X(t+1) = X_P(t) - A \cdot D. \tag{10}$$

The above equation captures the dynamic adjustment of each whale's position in the search space.

Key to this process are the variables A and C, which are defined as

$$\begin{aligned} A &= 2a \times r - a, \\ C &= 2r, \end{aligned} \tag{11}$$

where r represents a random number ranging between 0 and 1, and a linearly decreases from 2 to 0 over the course of the algorithm's iterations. The gradual decrease in a influences the scope of the search behavior, where t denotes the total number of iterations. The variable A controls the expansion and bracketing behavior of the algorithm's search agents: when the absolute value of A exceeds 1 ($|A| > 1$), the algorithm engages in a global search, exploring a wide range of the search space. Conversely, when $|A| < 1$, it conducts a local search, focusing on a more confined area to refine the solution.

(2) Predation phase (bubble-net attack)

In this phase, two hunting strategies of whales are simulated. The first strategy, the contraction cycle, gradually reduces the value of a in equation (11) from 2 to 0, mirroring the whale's encircling movement towards its prey. The second strategy, the spiral reupdate position, models the whale's spiral hunting motion. This is achieved by computing the distance D′ as per the following equation:

$$D' = \left| X_P(t) - X(t) \right|. \tag{12}$$

The new position is then updated using the following formulation:

$$X(t+1) = D' \times e^{\mathrm{bl}} \times \cos(2\pi l) + X_P(t), \tag{13}$$

where b is a constant, this paper takes 1, and l is any value in the interval [−1, 1]. The step D' represents the update distance during the predation process.

The whale adopts each strategy with an equal likelihood of 50%, as detailed in the following equation:

$$X(t+1) = \begin{cases} X_P(t) - A \cdot D, & P < 0.5, \\ D' \cdot e^{\mathrm{bl}} \cdot \cos(2\pi l) + X_P(t), & P \geq 0.5. \end{cases} \tag{14}$$

This approach effectively simulates the predatory behavior of whales, alternating between encircling and spiraling tactics to optimize the search process.

(3) Search phase

During this phase, the whales engage in a collaborative search across the solution space, randomly selecting and updating positions to enhance the algorithm's diversity and global search capabilities. This strategy helps prevent the algorithm from converging on the local optima, fostering more effective global optimization. The search process is detailed as follows:

$$D'' = \left| C \cdot X_{\mathrm{rand}}(t) - X(t) \right|, \tag{15}$$

where $X_{\mathrm{rand}}(t)$ represents a randomly selected solution.

2.4. Advancements in Neural Networks with DELM. The extreme learning machine (ELM) is a single hidden layer feedforward neural network algorithm characterized by the selection of random weights and thresholds. The unique aspect of ELM lies in its method of initializing these parameters randomly between the input layer and the hidden layer, and within the threshold matrix of the hidden layer. This approach effectively addresses the common issues in traditional backpropagation neural networks, where inappropriate initial weights and thresholds often lead to suboptimal local solutions [40]. Compared with traditional neural networks, DELM has shown a 5–10% higher accuracy in predicting structural deformations in concrete dams. The basic structure of ELM is shown in Figure 2.

The ELM model comprises three primary components: the input layer, the hidden (implicit) layer, and the output layer. The fundamental principle of ELM operates as follows: Let $X = \{x_i | 1 \leq i \leq N\}$ represent the input data sample set, and $Y = \{y_i | 1 \leq i \leq N\}$ denote the output data sample set, where N is the total number of samples, x_i is the i-th input sample, and y_i is the i-th output sample. In this setup, the hidden layer consists of J neurons, and $H = \{h_i | 1 \leq i \leq J\}$ is the set of output vectors of the hidden layer, with h_i being the feature vector corresponding to the i-th input sample. The output of the hidden layer is calculated by using the following equation:

$$H = G(\alpha X + B), \tag{16}$$

where G represents the activation function (which can be sigmoid, sin, and hardlim), α is the input weight matrix connecting each node in the input layer to each node in the hidden layer, and B is the threshold matrix for each node in the hidden layer.

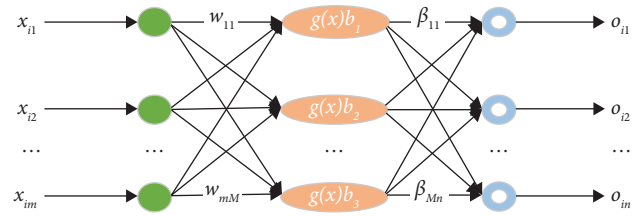

Figure 2: Schematic diagram of the ELM structure.

In scenarios where ELM with a single hidden layer closely approximates the output of N samples with minimal error, the output matrix of the hidden layer, H, is expressed as shown in the following equation:

$$H = \begin{bmatrix} g_i(\alpha_1 x_1) & \cdots & g_i(\alpha_J x_1 + b_J) \\ \vdots & \ddots & \vdots \\ g_i(\alpha_1 x_J + b_1) & \cdots & g_i(\alpha_J x_J + b_J) \end{bmatrix}, \tag{17}$$

where H is the implied layer output matrix.

The key advantage of DELM over traditional ELM is the incorporation of multiple hidden layers, enabling the construction of deep learning models that effectively capture significant features, thus enhancing learning and generalization capabilities. DELM is particularly recommended for data analysis, compensating for the limitations of ELM and incorporating regularization terms to further enhance the model's generalization potential. The output weight β in DELM is calculated by using the following equation:

$$\beta = \left(\frac{1}{C} + H^{\mathrm{T}} H \right)^{-1} H^{T} Y, \tag{18}$$

where C is the regularization factor.

In the ELM-AE framework, an autoencoder algorithm based on ELM, the model learns data features through unsupervised learning. It employs an encoder to map the input vector to the hidden layer and a decoder to reconstruct the feature vector back to the input. ELM-AE characteristically generates orthogonal random weights and thresholds:

$$\begin{aligned} \alpha^{\mathrm{T}} \alpha &= 1, \\ B^{\mathrm{T}} B &= 1. \end{aligned} \tag{19}$$

To further improve the generalization ability and robustness of ELM-AE, regularization coefficients are introduced. The objective function for least squares optimization is defined as

$$\min J_{\mathrm{ELM}} = \left\{ \frac{1}{2} \|\beta\|^2 + \frac{C}{2} \|Y - \beta H\|^2 \right\}, \tag{20}$$

where C is the regularization parameter. For sparse and compressed ELM-AE, the output weight β is determined by solving the equation:

$$\beta = \left(\frac{1}{C} + H^{\mathrm{T}} H \right)^{-1} H^{\mathrm{T}} X, \tag{21}$$

where H is the output matrix of the hidden layer of ELM-AE, and X is both the input and output of ELM-AE.

2.5. Deformation Trend Analysis. The methodology for analyzing dam deformation trends integrates VMD, fractal theory, and the WOA-DELM model. The detailed process, outlined in Figure 3, consists of the following steps:

Step 1: VMD of dam data

The initial step involves using the VMD method to decompose dam deformation data. This process yields the modal functions, their frequency spectra, and central frequencies, laying the foundation for further analysis. The specific initial parameter settings are as follows: the number of decomposition levels (K) is set to 7, the penalty factor is 2000, and the initial central frequency is set to 1.

Step 2: wavelet transform analysis

Upon obtaining the modal functions from VMD, the wavelet transform method is employed for further decomposition into wavelet packets. This step involves calculating local Hurst exponents and Katz functions for each modal function at various scales, providing a deeper understanding of the fractal characteristics of data. The preliminary settings are as follows: the wavelet decomposition employs the db4 wavelet basis, and the number of subsegments M is set to 5.

Step 3: construction of the WOA-DELM model

This critical phase focuses on constructing the WOA-DELM dam deformation prediction model using the VMD-processed data. The process involves several substeps:

(I) Normalization of data postnoise reduction.
(II) Setting parameters for the WOA-DELM model.
(III) Defining the fitness function for the model.
(IV) The WOA algorithm is first called for optimization to obtain the best weights and best fitness values for the DELM model. Then, the DELM model is trained using the best weights.
(V) The test data are then fed into the system, along with output weights and the implicit layer of ELM-AE, to compute predictions and validate the method.

The initial settings for the specific model are as follows: for the ELM-AE (extreme learning machine-autoencoder), the number of hidden layers is set to (60, 60, 60), with the activation function being "sigmoid." For the whale optimization algorithm, the number of whales in the population is 30, the maximum number of iterations is 20, the upper bound for the weights is 1, and the lower bound for the weights is −1.

Step 4: comparative analysis and model validation

The final step involves a comprehensive comparison between the model's predictions and the results obtained from wavelet transform analysis. By integrating the analytical results from the wavelet transform method and Katz function with the predictive outcomes, the analysis transcends from purely qualitative to a more robust quantitative evaluation. This improved approach allows for a more comprehensive and all-encompassing assessment of future dam deformation trends.

2.6. Engineering Context and Setup. This case study focuses on a significant hydropower project located along the middle reaches of the Lancang River in Yunnan Province. The project encompasses a range of structures, including a concrete double-curvature arch dam, a plunge pool, a secondary dam, a flood discharge tunnel, and an extensive underground water diversion and power generation system. The arch dam, a central feature of this project, stands at a height of 294.5 meters, maintains a normal water level of 1240 meters, and boasts an installed capacity of 4200 MW. It delivers a guaranteed output of 1778 MW and has an impressive annual generation capacity of 1.9 million kWh. An aerial view of the specific dam is shown in Figure 4.

To ensure the safety and optimal performance of the hydropower station, a comprehensive array of monitoring systems has been implemented. This includes an automated dam safety monitoring system, a global navigation satellite system-based deformation monitoring system for the dam crest, a three-dimensional laser measurement system, a dynamic monitoring system for seismic responses of the dam body, and a robust system for monitoring strong earthquakes. These systems are linked to over 6400 measuring points, making it China's most extensive and sophisticated automated safety monitoring system for high arch dams. Specifically, more than 6400 monitoring points include deformation monitoring, crack monitoring, seepage monitoring, temperature monitoring, and satellite monitoring. This paper mainly focuses on deformation monitoring. Therefore, 53 monitoring sites dedicated to deformation monitoring are selected in this paper. A detailed layout of these monitoring instruments is shown in Figure 5.

To assess the efficacy of the model under study, monitoring data from two specific points, C4-A22-PL-02 and C4-A22-PL-03, located on the arch crown beam of the double-curvature arch dam, have been selected as sample data. Figures 6 and 7 depict the displacement monitoring values, as well as the upstream and downstream water levels and air temperature readings, offering a comprehensive view of the dam's operational parameters.

3. Result Analysis: Hydropower Station Deformation Analysis

3.1. Noise Reduction and Signal Enhancement Using VMD. In this study, VMD is employed as a key method for noise reduction in the dam's measured data. The selection of the appropriate number of decomposition K values is a pivotal aspect of this process. Through various trials, the optimal value for K is determined to be 7. Alongside this, specific parameters are set, as shown in Table 1.

Figures 8 and 9 reveal noticeable fluctuations and outliers in the measured data. However, the application of VMD for noise reduction and data reconstruction significantly smoothens the displacement change curve, enhancing its

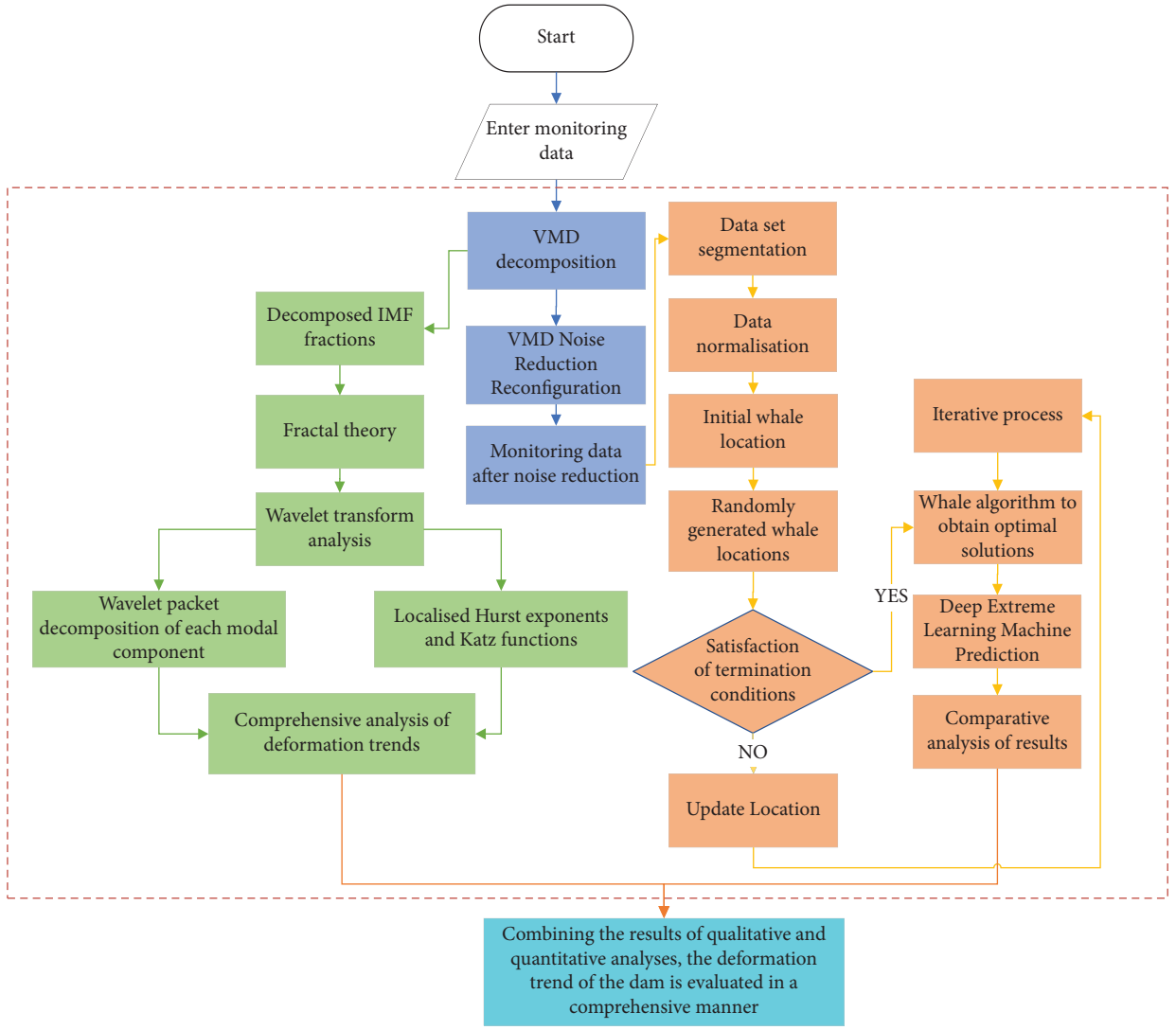

Figure 3: Integrated deformation trend analysis diagram.

(a) (b)

Figure 4: Aerial view of the dam: (a) downstream view and (b) upstream view.

coherence. This underscores the VMD algorithm's efficacy in eliminating abnormal noise and correcting data outliers. The refined data, devoid of noise and irregularities, facilitate a more precise analysis of trends and patterns. Consequently, the utilization of the VMD algorithm in processing monitoring data proves advantageous, yielding more reliable and accurate information essential for the assessment and management of dam operations.

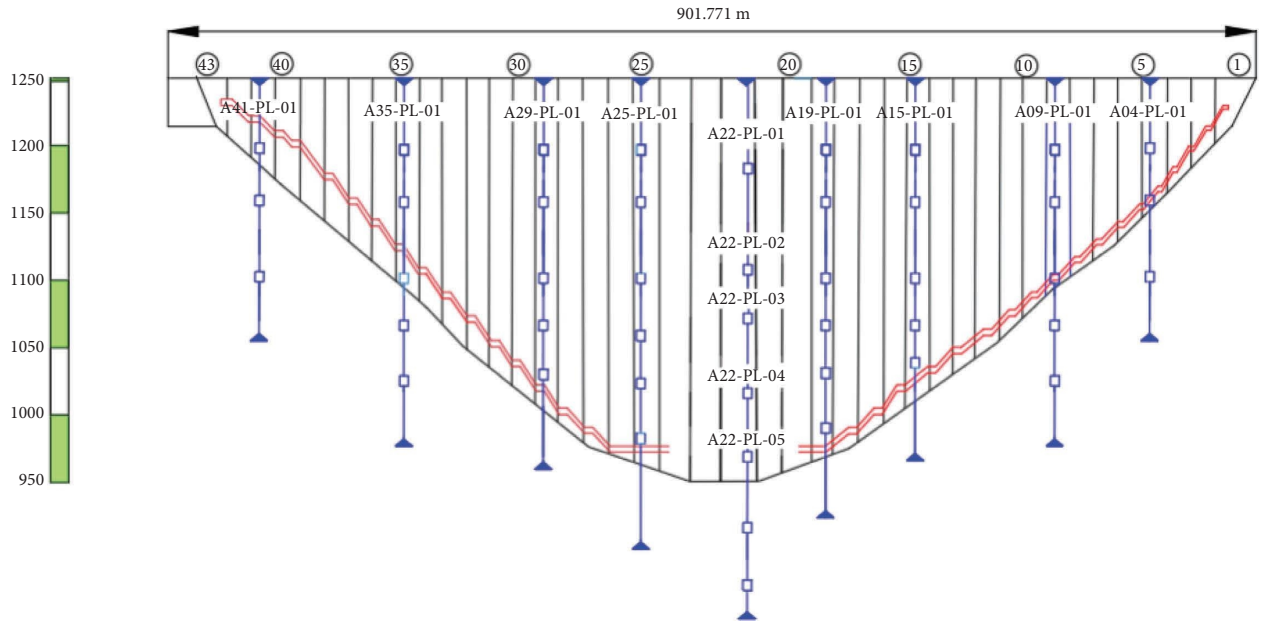

Figure 5: Layout of the pendulum monitoring instruments.

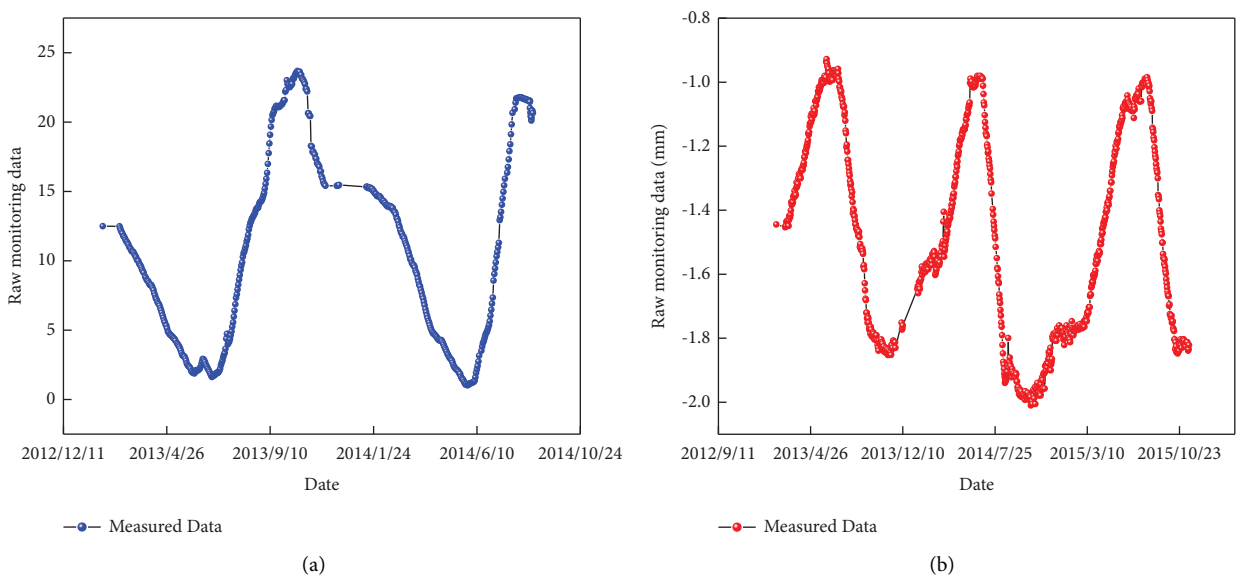

Figure 6: Displacement monitoring values for measurement points (a) C4-A22-PL-02 and (b) C4-A22-PL-03.

3.2. Analysis of Dam Deformation Using Fractal Theory. This section presents a detailed analysis of the deformation trends in a hydroelectric dam, utilizing data from the C4-A22-PL-02 and C4-A22-PL-03 monitoring points. The study employs the VMD method coupled with fractal theory tools, including wavelet transform analysis and the Katz function.

The monitoring data underwent decomposition into seven IMFs through VMD. Subsequently, each IMF was analyzed using WPD with the db4 wavelet basis. This approach facilitated the extraction of detailed information across various frequency and time domains. Key parameters such as the local Hurst exponent for each scale component were calculated, culminating in an overall Hurst exponent derived through a weighted average. This process was instrumental in assessing the long-term correlation characteristics of the deformation data. In addition, the Katz function was calculated for each IMF component, considering the signal length and the average step length. The results are shown in Table 2.

Analysis of Table 2 reveals that the Hurst exponent for each IMF component slightly varies, predominantly falling between 0.6 and 0.7. The overall Hurst exponent stands at 0.638, surpassing 0.5, which is indicative of a consistent upward trend in dam deformation at the monitored points. This trend is marked by a notable long-term correlation, regularity, and distinctiveness [41].

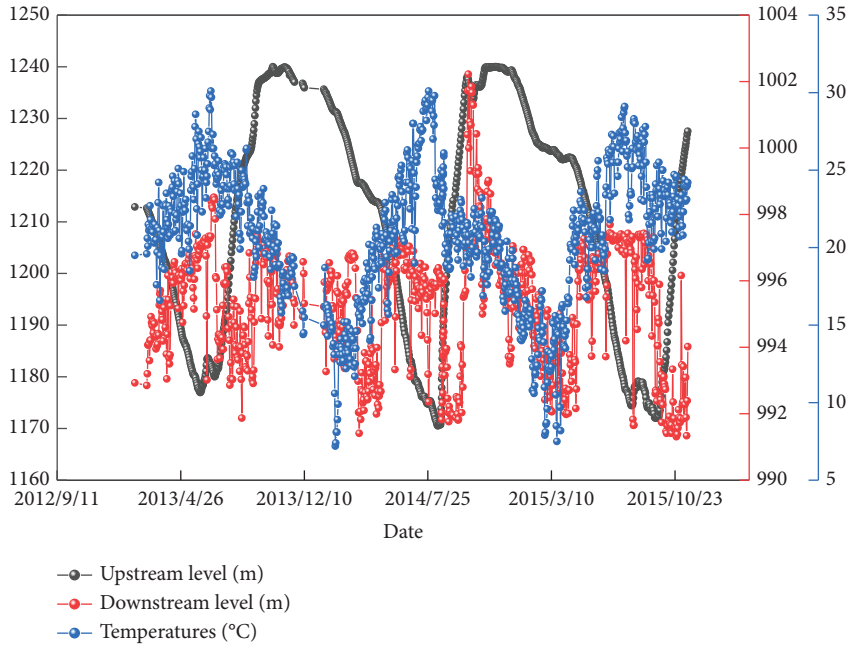

Figure 7: Dam upstream and downstream water levels and air temperature monitoring values.

Table 1: VMD setup parameters.

Parameter	Value
Number of decomposition levels (K)	7
Penalty factor	2000
Noise tolerance level	0
Direct current component	None
Initial center frequency	1
Convergence standard tolerance	0.0000001

Furthermore, the Katz function values, ranging from 0.349 to 0.385, denote minimal fluctuations in each signal component. The dam deformation monitoring data, therefore, exhibit a moderate level of long-term correlation over time. The overall Katz function value, at 0.403, suggests minimal variations in the signal within the context of dam deformation monitoring data, implying a consistent deformation trend with a moderate degree of long-term correlation.

Therefore, the analysis based on the Hurst exponent and Katz function values points towards a consistent and progressive upward trend in dam deformation at these monitoring points. The trend is characterized by stability and regularity, underlining the efficacy of this method in forecasting future deformation patterns. Our analysis aligns with Lin et al.'s [42] findings on deformation trends in arch dams, confirming the validity of our approach.

3.3. Evaluating the WOA-DELM Predictive Model. The WOA-DELM model's efficacy in predicting dam deformation trends is explored using a dataset comprising C4-A22-PL-02 and C4-A22-PL-03 monitoring data. In the monitoring dataset, time, upstream and downstream water levels, and temperature are used as input variables, and displacement is used as the output variable. The specific parameters of the WOA-DELM model are set as shown in Table 3.

To demonstrate the model's superiority in predicting dam deformation, a comparative analysis is conducted using DELM and LSTM models. This comparison, focusing on dam monitoring data post-VMD denoising, helps validate the WOA-DELM model's advantages. The prediction curves of each model are shown in Figure 10, and the residuals of the prediction model are shown in Figure 11.

The model's performance and accuracy are assessed using five metrics: goodness-of-fit (R^2), root mean square error (RMSE), mean absolute error (MAE), mean absolute percentage error (MAPE), and mean bias error (MBE). The specific model predictions are shown in Table 4.

4. Discussion

This study focuses on evaluating the long-term predictive capacity of the WOA-DELM model. For this purpose, the displacement data from measurement points C4-A22-PL-02 and C4-A22-PL-03 were used. Four distinct predictive models, WOA-DELM, WOA-LSTM, DELM, and LSTM, were developed after the VMD reconstruction of the monitoring data. The detailed reconstruction curves are depicted in Figure 9, prediction curves in Figure 10, residual box line diagrams in Figure 11, and the evaluation indices in Figures 12 and 13 and Table 4.

Observations from Figure 9 reveal the VMD process's effectiveness in enhancing data quality. The VMD approach not only smoothens the signals but also retains crucial edge information, thus preserving the integrity and characteristics of the original dataset. This leads to a more authentic representation of the dam's deformation patterns.

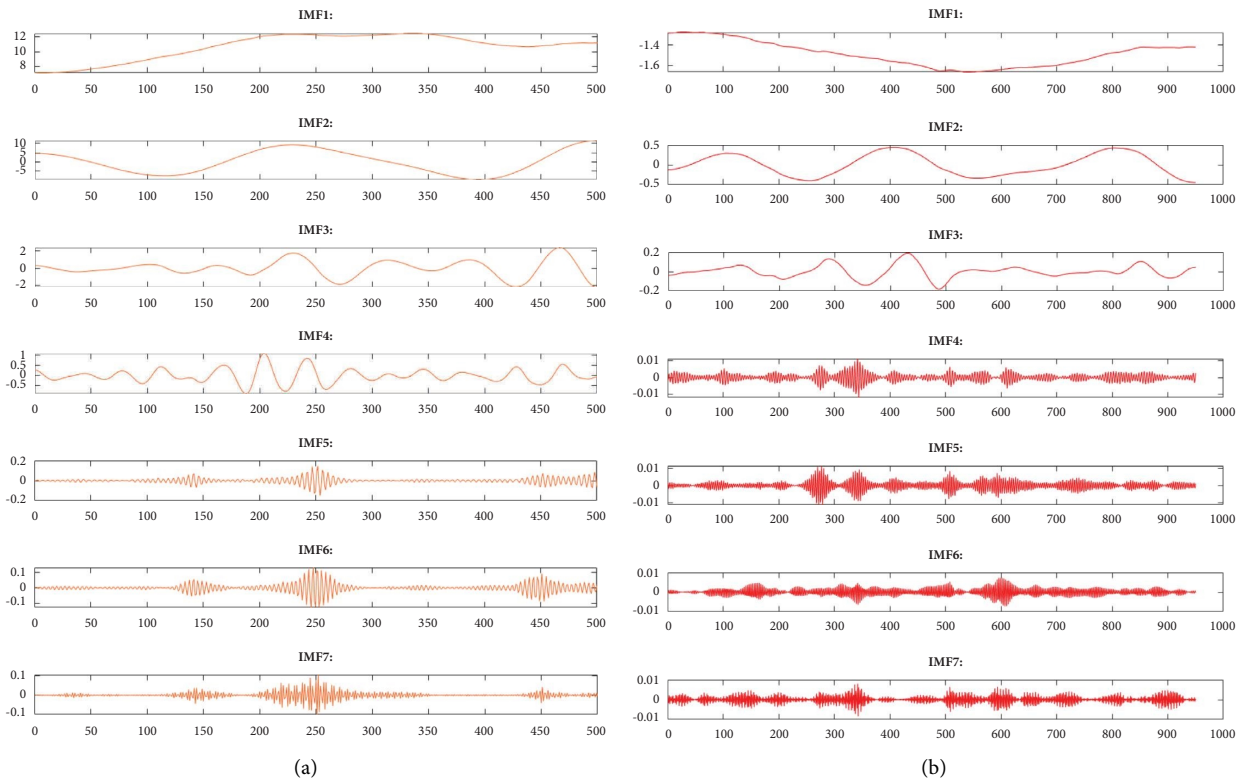

Figure 8: VMD decomposition of IMF components: (a) C4-A22-PL-02 and (b) C4-A22-PL-03.

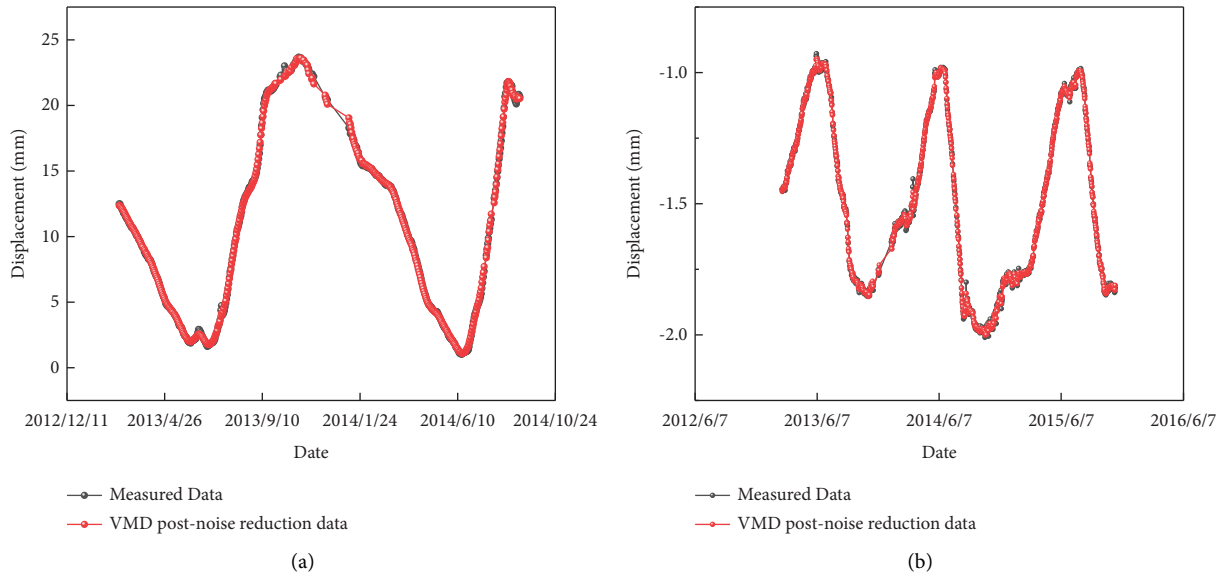

Figure 9: Monitoring values post-VMD processing for measurement points (a) C4-A22-PL-02 and (b) C4-A22-PL-03.

Table 2: Results from fractal theory analysis.

	IMF1	IMF2	IMF3	IMF4	IMF5	IMF6	IMF7	IMF overall
Hurst index	0.642	0.644	0.643	0.641	0.636	0.626	0.628	0.638
Katz dimension	0.349	0.385	0.372	0.367	0.371	0.384	0.385	0.403

Table 3: Parameter settings for the WOA-DELM model.

Parameter	Value
ELM-AE hidden layer	(60, 60, 60)
Activation function	"Sig"
C	Inf
Population size	30
Maximum number of iterations	20
Lower bound	−1
Upper bound	1

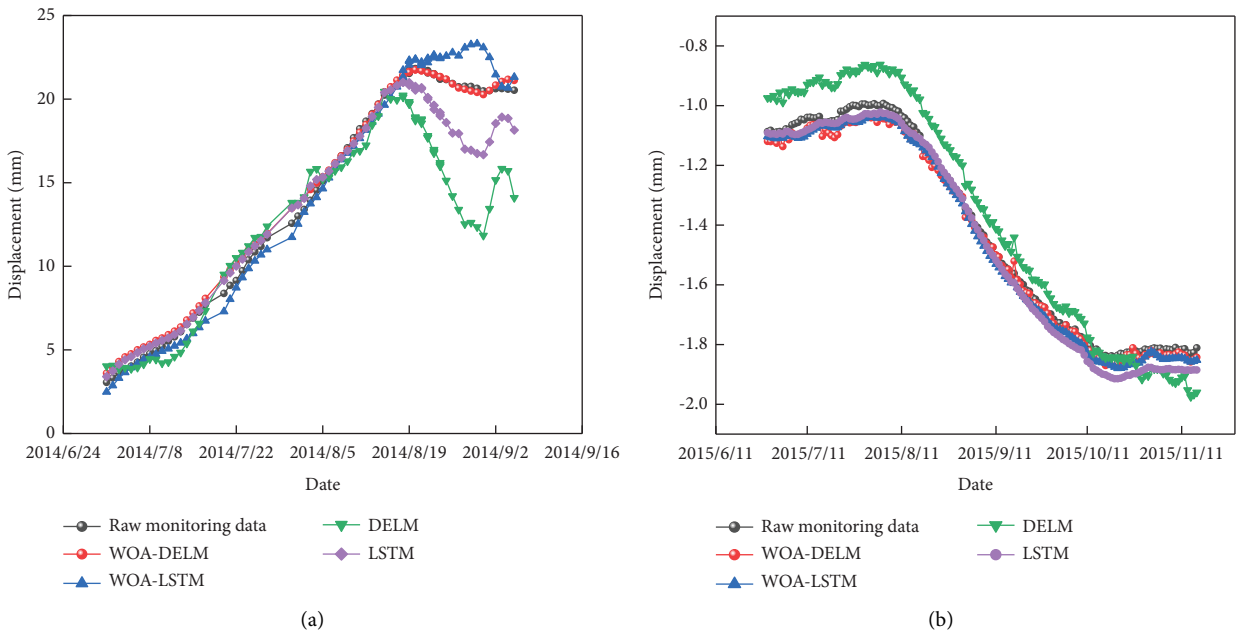

Figure 10: Comparative prediction results for (a) C4-A22-PL-02 and (b) C4-A22-PL-03.

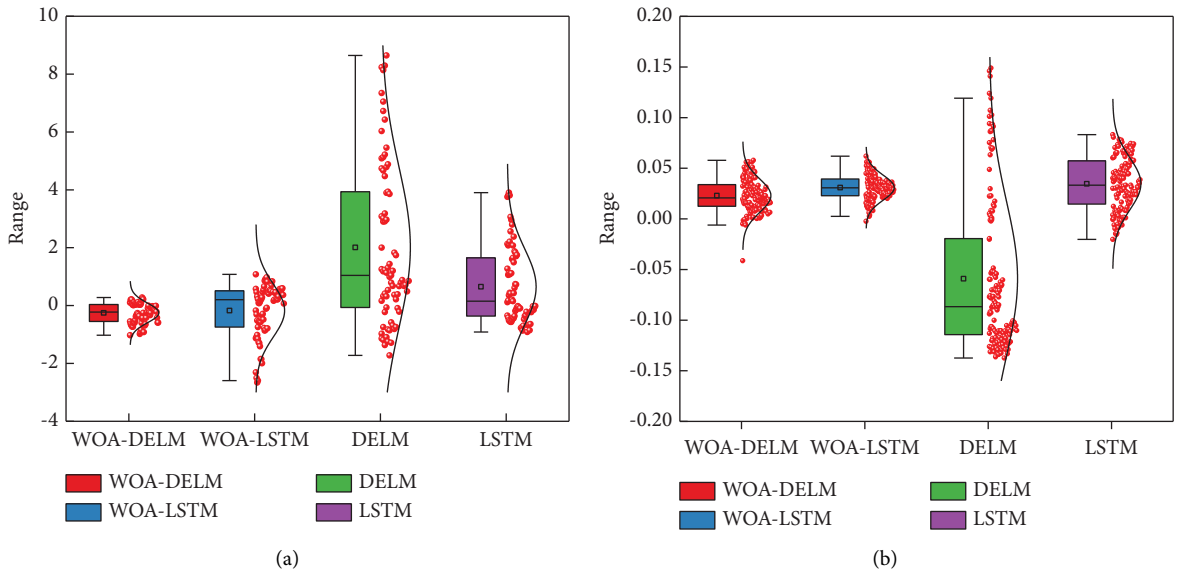

Figure 11: Residual box line diagrams for prediction models at (a) C4-A22-PL-02 and (b) C4-A22-PL-03.

Table 4: Prediction results of the models.

		RMSE	MAE	MAPE	MBE
C4-A22-PL-02	WOA-DELM	0.421	0.319	0.037	0.253
	WOA-LSTM	0.925	0.711	0.054	0.648
	DELM	3.407	2.434	0.186	2.011
	LSTM	1.45	1.027	0.07	0.649
C4-A22-PL-03	WOA-DELM	0.028	0.019	0.024	0.023
	WOA-LSTM	0.033	0.024	0.031	0.031
	DELM	0.098	0.073	0.091	0.057
	LSTM	0.044	0.026	0.038	0.036

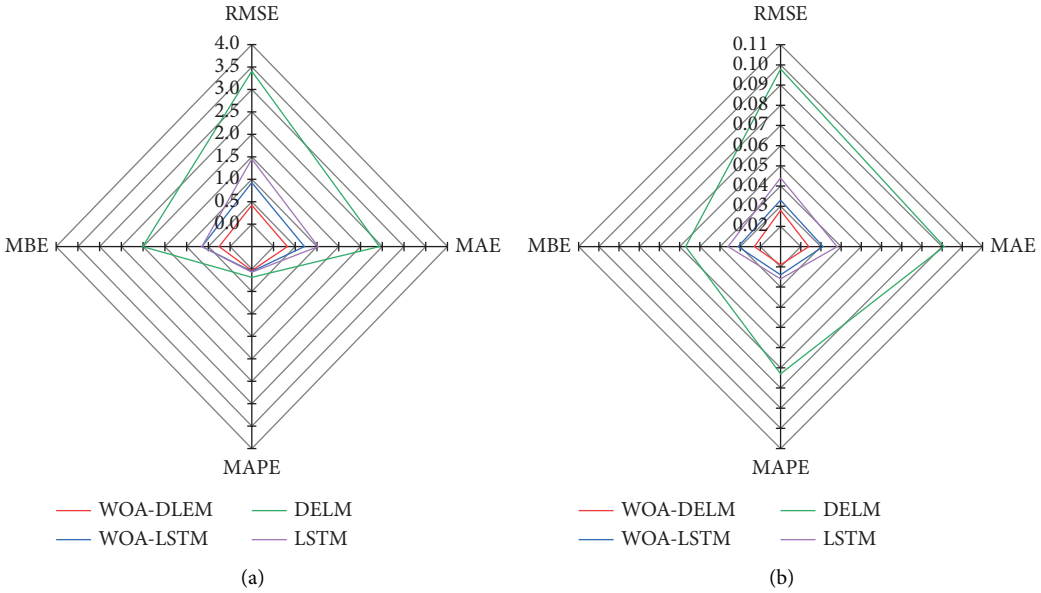

Figure 12: Model performance indicators for (a) C4-A22-PL-02 and (b) C4-A22-PL-03.

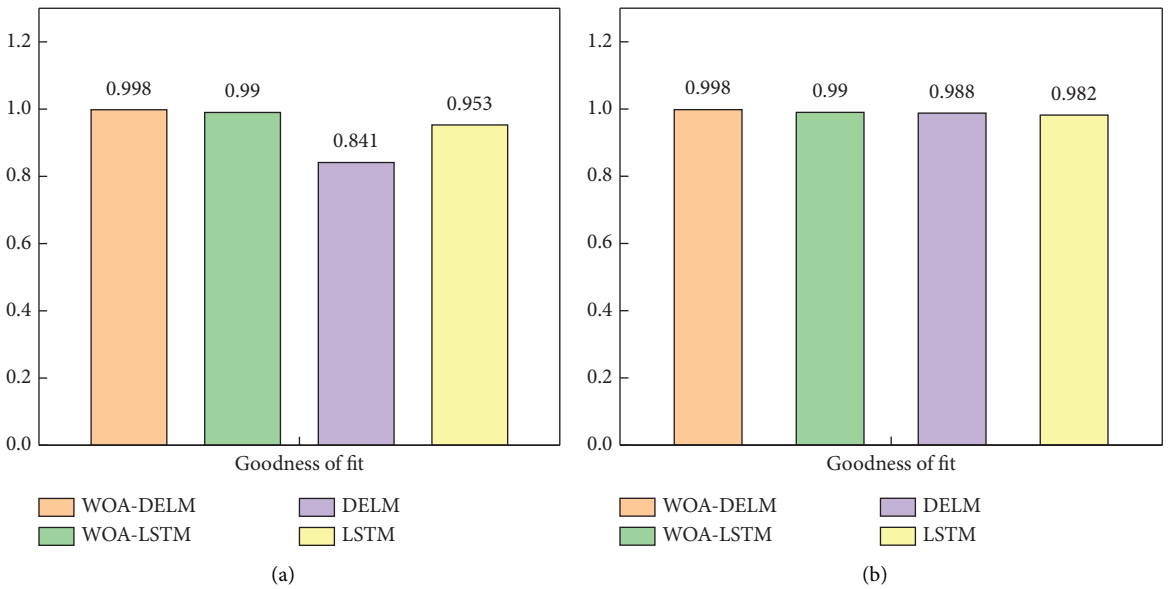

Figure 13: Model goodness-of-fit for (a) C4-A22-PL-02 and (b) C4-A22-PL-03.

A closer examination of Figures 10–13 and Table 4 illustrates the superior performance of the WOA-DELM model. The model demonstrates the highest R^2 and the smallest values in RMSE, MAE, MAPE, and MBE across different measurement points, where R^2 is used to measure how well the model fits the data. RMSE measures the average difference between the predicted and true values of the model. MAE is the mean of the absolute values of the prediction errors. MAPE is the mean of the prediction errors expressed as a percentage. MBE measures the systematic bias of the predicted values of the model. This comparison highlights the model's robustness and precision in predicting dam deformations.

Furthermore, Figure 11 indicates minimal fluctuations in the WOA-DELM model's residual values, typically ranging between 0 and 0.05. This is notably lower compared to the residual values observed in the WOA-LSTM, DELM, and LSTM models, thereby underscoring the WOA-DELM model's consistency and reliability.

Correlating the model predictions with the actual deformation trend, as shown in Figure 10, reveals a steady negative growth pattern in the dam's displacement over approximately 90 days. This trend is consistent with the deformation analysis using VMD and fractal theory, as outlined in Table 1. The convergence of findings from both predictive and analytical approaches affirms a sustained negative growth in dam deformation, aligning with real-world engineering observations.

This comprehensive analysis not only confirms the effectiveness of fractal theory in qualitative assessments but also validates the reliability of the WOA-DELM model in predictive scenarios. The integration of fractal theory with the WOA-DELM model for dam deformation trend analysis exemplifies a robust and effective approach for predicting and understanding dam dynamics.

5. Conclusion

This research has developed a comprehensive analytical framework aimed at an in-depth analysis of dam deformation trends. The framework integrates VMD for noise reduction, fractal theory analysis, and the WOA-DELM models. The VMD technique plays a pivotal role in eliminating noise from actual measured data, while the wavelet transform analysis method and Katz function from fractal theory are utilized for an in-depth qualitative analysis of the modal components derived from VMD. This approach, which combines both qualitative and quantitative analyses, significantly enhances the precision in identifying dam deformation trends.

Based on this, the deep extreme learning machine (DELM) is selected as the base model, which is then optimized using the whale optimization algorithm (WOA) to form the efficient WOA-DELM model. This model plays a crucial role in characterizing dam deformation trends, and its predictive outcomes are meticulously compared and analyzed against the results of fractal theory to verify their accuracy.

The proposed comprehensive model significantly preserves the original form and characteristics of the data during the noise reduction process. By applying fractal theory to analyze the VMD modal components, the model can more accurately identify the deformation trends of the dam. The introduction of the WOA-DELM model not only validates these trends but also provides an innovative methodology for analyzing dam deformation trends.

Despite the model's significant contributions, it also has limitations that point to future research directions. The dependency on high-precision data acquisition highlights the importance of advanced equipment for capturing detailed and accurate data. While the VMD method is effective, it faces challenges when dealing with complex signals, indicating a need for further refinement. In addition, a more rigorous method is required to verify the consistency of the model's predictive results with the findings from fractal theory analysis, ensuring the consistency and reliability of the results.

Future research will focus on enhancing monitoring data processing technology by exploring new intelligent algorithms to better analyze the intrinsic characteristics of dam monitoring data. At the same time, innovative data acquisition techniques will be developed to collect higher quality and more comprehensive monitoring data, thereby enhancing the ability of monitoring data processing technology to handle complex signals. In addition, the use of fractal theory to construct corresponding models will allow for a more accurate description and prediction of dam deformation behavior. Continuous optimization of the WOA-DELM model will further improve monitoring efficiency. These research efforts will provide more accurate, reliable, and applicable solutions for analyzing dam deformation trends, thereby strengthening the safety and operational integrity of dams.

Data Availability

The data used to support the findings of this study are available from the corresponding author upon request.

Conflicts of Interest

The authors declare that they have no conflicts of interest.

Acknowledgments

This work was financially supported by the National Natural Science Foundation of China (Grant nos. 52069029, 52079120, and 52369026).

References

[1] D. Y. Yuan, B. W. Wei, B. Xie, and Z. M. Zhong, "Modified dam deformation monitoring model considering periodic component contained in residual sequence," *Structural Control and Health Monitoring*, vol. 27, no. 12, 2020.

[2] R. Y. Yuan, C. Su, E. H. Cao, S. P. Hu, and H. Zhang, "Exploration of multi-scale reconstruction framework in dam

deformation prediction," *Applied Sciences*, vol. 11, no. 16, 2021.

[3] H. Z. Su, X. Q. Yan, H. P. Liu, and Z. P. Wen, "Integrated multi-level control value and variation trend early-warning approach for deformation safety of arch dam," *Water Resources Management*, vol. 31, no. 6, pp. 2025–2045, 2017.

[4] Q. B. Ren, M. C. Li, L. G. Song, and H. Liu, "An optimized combination prediction model for concrete dam deformation considering quantitative evaluation and hysteresis correction," *Advanced Engineering Informatics*, vol. 46, Article ID 101154, 2020.

[5] Y. J. Zeng, J. W. Zhang, D. G. Cao, and H. K. Wu, "Application of RS-RF model in deformation prediction of concrete dam," *Water Resources and Hydropower Technology (English and Chinese)*, vol. 52, no. 05, pp. 82–88, 2021.

[6] J. Hu and F. H. Ma, "Comparison of hierarchical clustering based deformation prediction models for high arch dams during the initial operation period," *Journal of Civil Structural Health Monitoring*, vol. 11, no. 4, pp. 897–914, 2021.

[7] B. W. Wei, S. Y. Luo, F. G. Xu, H. K. Li, L. J. Chen, and B. Liu, "Hybrid model for concrete dam deformation in consideration of residual correction by frequency division," *Structural Control and Health Monitoring*, vol. 29, no. 6, 2022.

[8] J. Hu and F. H. Ma, "Statistical modelling for high arch dam deformation during the initial impoundment period," *Structural Control and Health Monitoring*, vol. 27, no. 12, 2020.

[9] S. W. Wang, C. Xu, Y. Liu, and B. B. Wu, "Mixed-coefficient panel model for evaluating the overall deformation behavior of high arch dams using the spatial clustering," *Structural Control and Health Monitoring*, vol. 28, no. 10, 2021.

[10] X. N. Qin, C. S. Gu, B. Chen, C. G. Liu, B. Dai, and Y. L. Yu, "Multi-block combined diagnosis indexes based on dam block comprehensive displacement of concrete dams," *Optik*, vol. 129, pp. 172–182, 2017.

[11] B. W. Wei, L. J. Chen, H. K. Li, D. Y. Yuan, and G. Wang, "Optimized prediction model for concrete dam displacement based on signal residual amendment," *Applied Mathematical Modelling*, vol. 78, pp. 20–36, 2020.

[12] S. W. Wang, C. Xu, Y. Liu, and B. B. Wu, "A spatial association-coupled double objective support vector machine prediction model for diagnosing the deformation behaviour of high arch dams," *Structural Health Monitoring*, vol. 21, no. 3, pp. 945–964, 2022.

[13] E. H. Cao, T. F. Bao, H. Li et al., "A hybrid feature selection-multidimensional LSTM framework for deformation prediction of super high arch dams," *KSCE Journal of Civil Engineering*, vol. 26, no. 11, pp. 4603–4616, 2022.

[14] X. D. Chen, Z. H. Chen, S. W. Hu, C. S. Gu, J. J. Guo, and X. N. Qin, "A feature decomposition-based deep transfer learning framework for concrete dam deformation prediction with observational insufficiency," *Advanced Engineering Informatics*, vol. 58, Article ID 102175, 2023.

[15] S. Deng, L. T. Y Zhou, and Z. K. Liu, "Analysis method of dam deformation trend based on Kalman filter, fractal and LSTM," *Advances in Science and Technology of Water Resources*, vol. 42, no. 05, pp. 121–126, 2022.

[16] Y. H. Hao, Y. Y. Hao, C. Z. Tang, and H. Yang, "Research on dam deformation trend judgment and prediction based on deformation information decomposition," *Journal of Geodesy and Geodynamics*, vol. 41, no. 08, 2021.

[17] K. T. T. Bui, J. F. Torres, D. Gutiérrez-Avilés, V. H. Nhu, D. T. Bui, and F. Martínez-Álvarez, "Deformation forecasting of a hydropower dam by hybridizing a long short-term memory deep learning network with the coronavirus optimization algorithm," *Computer-Aided Civil and Infrastructure Engineering*, vol. 37, no. 11, pp. 1368–1386, 2022.

[18] E. H. Cao, T. F. Bao, C. S. Gu, H. Li, Y. T. Liu, and S. P. Hu, "A novel hybrid decomposition—ensemble prediction model for dam deformation," *Applied Sciences*, vol. 10, no. 16, p. 5700, 2020.

[19] Q. F. Zhang, S. Chen, and Z. P. Fan, "Bearing fault diagnosis based on improved particle swarm optimized VMD and SVM models," *Advances in Mechanical Engineering*, vol. 13, no. 6, 2021.

[20] Y. S. Liu, J. S. Kang, L. Wen, Y. J. Bai, and C. M. Guo, "Health status assessment of diesel engine valve clearance based on BFA-BOA-VMD adaptive noise reduction and multi-channel information fusion," *Sensors*, vol. 22, no. 21, 2022.

[21] Z. A. Chen, X. Xiong, and Y. Y. You, "Variational mode decomposition and long short-term neural network for dam deformation prediction," *Science Surveying and Mapping*, vol. 46, no. 09, pp. 34–42, 2021.

[22] W. C. Wang, B. Wang, K. W. Chau, Y. W. Zhao, H. F. Zang, and D. M. Xu, "Monthly runoff prediction using gated recurrent unit neural network based on variational modal decomposition and optimized by whale optimization algorithm," *Environmental Earth Sciences*, vol. 83, no. 2, 2024.

[23] D. M. Xu, X. Wang, W. C. Wang, K. W. Chau, and H. F. Zang, "Improved monthly runoff time series prediction using the SOA–SVM model based on ICEEMDAN–WD decomposition," *Journal of Hydroinformatics*, vol. 25, no. 3, pp. 943–970, 2023.

[24] C. T. Yang, R. D. Huang, D. W. Liu, W. C. Qiu, R. P. Zhang, and Y. Tang, "Analysis and warning prediction of tunnel deformation based on multifractal theory," *Fractal and Fractional*, vol. 8, no. 2, 2024.

[25] H. Z. Su, Z. P. Wen, F. Wang, and J. Hu, "Dam structural behavior identification and prediction by using variable dimension fractal model and iterated function system," *Applied Soft Computing*, vol. 48, pp. 612–620, 2016.

[26] Y. H. Xiang, F. Zhang, N. W. Deng, and Y. H. Xie, "Dam deformation analysis based on hybrid model of fractal interpolation and support vector machine," *China Rural Water and Hydropower*, vol. 185, no. 01, pp. 188–193, 2023.

[27] Y. H. Xie, N. W. Deng, and Y. J. Liu, "Analysis and prediction of the dam deformation based on multifractal principle," *Hydropower and New Energy*, vol. 35, no. 04, pp. 32–37, 2021.

[28] W. T. Liu, Y. Y. Ren, X. X. Meng, B. Tian, and X. H. Lv, "Analysis of potential water inflow rates at an underground coal mine using a WOA-CNN-SVM approach," *Water*, vol. 16, no. 6, 2024.

[29] Y. R. Xu, Z. M. Xu, J. Ye, and Z. F. Zhang, "Estimation of road friction coefficient based on WOA-BP neural network," *Proceedings of the Institution of Mechanical Engineers-Part D: Journal of Automobile Engineering*, vol. 0, no. 0, 2024.

[30] Y. T. Li, Y. Zeng, J. Qian, F. J. Yang, and S. H. Xie, "Parameter identification of DFIG converter control system based on WOA," *Energies*, vol. 16, no. 6, 2023.

[31] Y. Dai, J. Pang, X. K. Rui, W. W. Li, Q. H. Wang, and S. K. Li, "Thermal error prediction model of high-speed motorized spindle based on DELM network optimized by weighted mean of vectors algorithm," *Case Studies in Thermal Engineering*, vol. 47, Article ID 103054, 2023.

[32] J. Lai, X. D. Wang, Q. Xiang, Y. F. Song, and W. Quan, "Multilayer discriminative extreme learning machine for classification," *International Journal of Machine Learning and Cybernetics*, vol. 14, no. 6, pp. 2111–2125, 2023.

[33] K. Dragomiretskiy and D. Zosso, "Variational mode decomposition," *IEEE Transactions on Signal Processing*, vol. 62, no. 3, pp. 531–544, 2014.
[34] Y. Han, L. H. Wang, P. H. Wei, Z. D. Li, and W. X. Zhou, "VMD-CNN-GRU hybrid prediction model of reservoir water level," *Journal of Nanjing University of Information Science and Technology*, vol. 16, no. 2, pp. 239–246, 2023.
[35] L. Pei, J. K. Chen, J. R. Zhou et al., "A fractal prediction method for safety monitoring deformation of core rockfill dams," *Mathematical Problems in Engineering*, vol. 11, 2021.
[36] K. J. Sharkey, "A control analysis perspective on Katz centrality," *Scientific Reports*, vol. 7, no. 1, Article ID 17247, 2017.
[37] X. G. Yang, Y. Zhang, and X. J. Li, "Abnormal noise identification of engines based on wavelet packet transform and bispectrum analysis," *Advances in Mechanical Engineering*, vol. 16, no. 1, 2024.
[38] H. R. Wang, X. Q. Niu, L. F. Xu, T. Y. Yan, and Y. T. Zhu, "Dam deformation prediction model based on singular spectrum analysis and improved whale optimization algorithm-optimized BP neural network," *Journal of Hydroelectric Engineering*, vol. 42, no. 11, pp. 136–145, 2023.
[39] S. Mirjalili and A. Lewis, "The whale optimization algorithm," *Advances in Engineering Software*, vol. 95, pp. 51–67, 2016.
[40] X. H. Zhu, X. M. She, Z. W. Ni, P. F. Xia, and C. Zhang, "Coke price prediction based on ELM optimized by double-elite evolution salp swarm algorithm," *Computer Science*, vol. 50, no. 05, pp. 292–301, 2023.
[41] X. C. Zhang, L. X. Chen, and C. Zhou, "Deformation monitoring and trend analysis of reservoir bank landslides by combining time-series InSAR and Hurst index," *Remote Sensing*, vol. 15, 2023.
[42] C. Lin, Y. Zou, X. H. Lai, X. Y. Wang, and Y. Su, "Variation trend prediction of dam displacement in the short-term using a hybrid model based on clustering methods," *Applied Sciences*, vol. 13, no. 19, Article ID 10827, 2023.